



This is a repository copy of *In situ formation of 1D nanostructures from ceria nanoparticle dispersions by liquid cell TEM irradiation*.

White Rose Research Online URL for this paper:  
<https://eprints.whiterose.ac.uk/153685/>

Version: Published Version

---

**Article:**

Asghar, M.S.A., Inkson, B.J. [orcid.org/0000-0002-2631-9090](https://orcid.org/0000-0002-2631-9090) and Möbus, G. (2020) In situ formation of 1D nanostructures from ceria nanoparticle dispersions by liquid cell TEM irradiation. *Journal of Materials Science*, 55 (7). pp. 2815-2825. ISSN 0022-2461

<https://doi.org/10.1007/s10853-019-04140-0>

---

**Reuse**

This article is distributed under the terms of the Creative Commons Attribution (CC BY) licence. This licence allows you to distribute, remix, tweak, and build upon the work, even commercially, as long as you credit the authors for the original work. More information and the full terms of the licence here:  
<https://creativecommons.org/licenses/>

**Takedown**

If you consider content in White Rose Research Online to be in breach of UK law, please notify us by emailing [eprints@whiterose.ac.uk](mailto:eprints@whiterose.ac.uk) including the URL of the record and the reason for the withdrawal request.



[eprints@whiterose.ac.uk](mailto:eprints@whiterose.ac.uk)  
<https://eprints.whiterose.ac.uk/>



# In situ formation of 1D nanostructures from ceria nanoparticle dispersions by liquid cell TEM irradiation

M. S. A. Asghar<sup>1</sup>, B. J. Inkson<sup>1</sup>, and G. Möbus<sup>1,\*</sup>

<sup>1</sup>Department of Materials Science and Engineering, University of Sheffield, Sheffield, UK

Received: 14 June 2019

Accepted: 16 October 2019

© The Author(s) 2019

## ABSTRACT

Deliberate electron irradiation of cerium oxide nanoparticles in water is used to trigger chemical reactions in a liquid cell transmission electron microscope. Formation of nanorods and nanoneedles is observed starting from predominantly octahedral shape nanoparticles. Detailed morphologies found include free-standing needles, needles connected to specific octahedral ceria facets and star-shaped multi-needle patterns. It is found that rod-axis orientations and crystallographic directions are aligned. It is suggested that high ion and radical concentration of radiolysed water dissolves layers of the original CeO<sub>2</sub> particles which re-arrange as needles in the direction of energetically preferred facets.

## Introduction

Ceria nanoparticles are involved directly or indirectly in a variety of nanoengineering and biomedical applications due to their exceptional properties [1]. Many applications of ceria nanoparticles rely on the ability to change oxidation state between 3+ and 4+, and a particularly large range of applications uses the particles in water or water vapour. Examples include applications for ultraviolet blocking in liquid sun screens, for biomedical radiation protection applications in cellular fluid [2], and most prominently as a catalytic material, e.g. for the water gas shift reaction, solar thermochemical water splitting, conversion of organic pollutants in water and in automotive catalytic converters [3].

There are many facile synthesis methods available for ceria nanoparticles such as laser-induced, hydrothermal, solvothermal and chemical

precipitation synthesis, next to thermal decomposition, and various sol-gel procedures [1, 3]. For controlling size, morphology/shape and dimensionality of nanoceria in colloidal dispersions either variation in anion concentration, temperature and pH or structure directing organic additives or templates have been used [4–6]. Particular recent interest focuses on the promotion of one-dimensional growth of ceria nanostructures, such as nanorods [7, 8].

The origin of self-assembly of nanoparticles in a polar liquid is thought to be a combination of long-range electrostatic and dipole-dipole forces in nanocolloids, where particles are embedded in double-layer charge shells [9, 10]. Upon closest approach, a competition between attractive van der Waals forces and repulsive forces from hydration layers arises [11, 12]. Most of these forces are non-directional leading to 2D/3D assembly of particles. The main exceptions are the dipole forces, which have been

Address correspondence to E-mail: g.moebus@sheffield.ac.uk

modelled to be essential for 1D chain formation [12]. Dispersion and particle attraction are heavily dependent on surface functionalisation, e.g. via oligomer shells [10]. Movement, agglomeration and deagglomeration of ceria NPs in liquid are very sensitive to any change in their physicochemical environment conditions such as pH, ionic strength, temperature and concentration of NPs [10, 13]. Reactions of ceria in water or with an adsorbed water vapour layer or molecule are industrially important (e.g. [14]), but difficult to examine experimentally on the atomic scale, therefore *ab initio* modelling is frequently applied [15, 16]. Historically, it has been difficult to track the mechanisms of particle synthesis and colloidal assembly methods without opportunity of live observations. However, the recently developed methodology of liquid cell transmission electron microscopy (TEM) enables *in situ* wet observation of particles [17].

Some particularly relevant recent literature with respect to our work is the growth of Cu<sub>2</sub>O shell phase on pre-existing Au nanoparticles from a Cu sulphate solution within liquid cell TEM [18], the trade-off between growth and dissolution of Au particles found for liquid cell TEM [19], and finally the *in situ* attachment of oxide nanoparticles to pre-existing 1D fibres is explored [20].

Here, we aim at real-time observation of ceria 1D assembly processes in aqueous systems triggered by rapidly and locally changing pH and water ionisation around ceria nanoparticles due to electron irradiation in TEM, in continuation of our recent studies on particle corrosion [21, 22].

## Materials and methods

Dispersions of commercial ceria nanoparticles in deionised (DI) water have been investigated, which have an approximate size of 10–40 nm (CeO<sub>2</sub>, purity > 99.9%, Sigma Aldrich, UK). The TEM liquid cell holder, Protochips Inc. USA [23], comprises a microfluidic silicon cell, with two silicon nitride membranes separated by a spacer of nominally 500 nm height and sealed by vacuum O-rings. The silicon nitride electron transparent membranes are plasma cleaned to make a hydrophilic surface. After loading into the TEM, additional small amounts of liquid can be added from a manual glass syringe,

filled with DI water, through internal tubing into the TEM holder.

For concurrent electron irradiation, real-time TEM liquid cell imaging and *in situ* video recording we have used a JEOL JEM 3010 transmission electron microscope operated at 300 kV with LaB<sub>6</sub> cathode and Tietz/TVIPS video-rate digital CCD camera, operating up to 30 fps, used here at around 6fps. The irradiation dose used is as reported before [21] and comprises an increase of intensity through beam convergence until a reactive regime is reached, when about exceeding  $\approx 3 \text{ nA}/\mu\text{m}^2$ . The individual conditions will however depend on water thickness, which varies from the above nominal thickness by membrane bending (underestimation) or by water evaporation (overestimation).

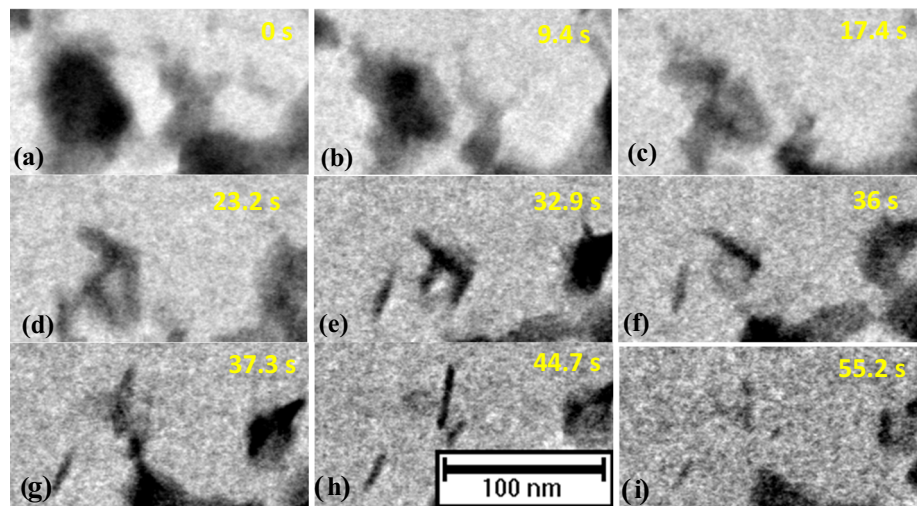
## Results

Under high-intensity electron irradiation, the main observation of liquid cell TEM of ceria particles is their surprisingly fast dissolution, details of which have been reported recently [21, 22]. However, in parallel to this primary dissolution tendency, here we report about materials transformations, including a variety of new shapes. We track and analyze the formation of new 1D objects, including individual needles, needles attached to particles, needles connecting pairs of particles and finally chains of particles. All of these new findings are still considered to be part of the overall corrosional scenario, as the major observations are not made before at least some corrosion attack has modified the primary particles.

### Formation of 1D nanostructures

The first scenario, “case 1” as of Fig. 1, comprises the formation of needle morphologies, free standing and supported only by the Si<sub>3</sub>N<sub>4</sub> membrane. This development of new phase of needle morphology has been briefly reported [21] but not examined and explained; The timing is parallel to the radiolytic dissolution processes of original octahedral ceria nanoparticles, which is described in Asghar et al. [22], and is not dependent on the continued existence of raw faceted ceria nanoparticles. The mass-thickness contrast of newly formed needles is similar to raw ceria, and their crystalline nature is deduced from their straight axis, their flat facets and Bragg scattering features

**Figure 1** Generation and transformation of needle-shaped particles. Case 1: Formation of needles free-standing on the support membrane.



visible. Figure 1a–i shows various stages of needle formation, starting from equal aspect particles of size close to original (Fig. 1a, b) over rectangular particles (Fig. 1c–d), needles of increasing sharpness (Fig. 1e–h), and finally needle dissolution (Fig. 1g). During intermediate stages (Fig. 1b, c), the solid crystalline matter appears surrounded by amorphous matter, as discussed in Asghar et al. [21], possibly related to amorphous hydroxide phase.

However, more common than those free-standing needles are occasions where new needles form from existing solid particles, in well-defined geometric orientation, and remaining attached. This is the “case 2”, tracked in Fig. 2. Formation of needles starts as rather broad pyramids on two particles changing the original octahedral shape via corner sharpening. The yellow pair of arrows tracks an octahedral corner turning pyramidal, while the blue pair tracks a pyramidal corner turning needle shape, becoming sharper and pointier, increasing their aspect ratio (Fig. 2a–d). The evidence shows that needles preferentially grow parallel to a central mirror plane of the particles. In our earlier work [24, 25], these particles predominantly showed {100} capped cube–octahedral shapes: Combining these two sets of information, the needles seem form preferentially on {100} nanofacets along  $\langle 100 \rangle$  orientation. Evidently, the needles are themselves subject to radiolytic dissolution and therefore exist temporarily. However, the fact that after significant irradiation and raw particle dissolution, the needles become more prominent and visible across the viewing area, indicates an enrichment of needle phase relative to original particles, or a conversion of original particles into needle phase,

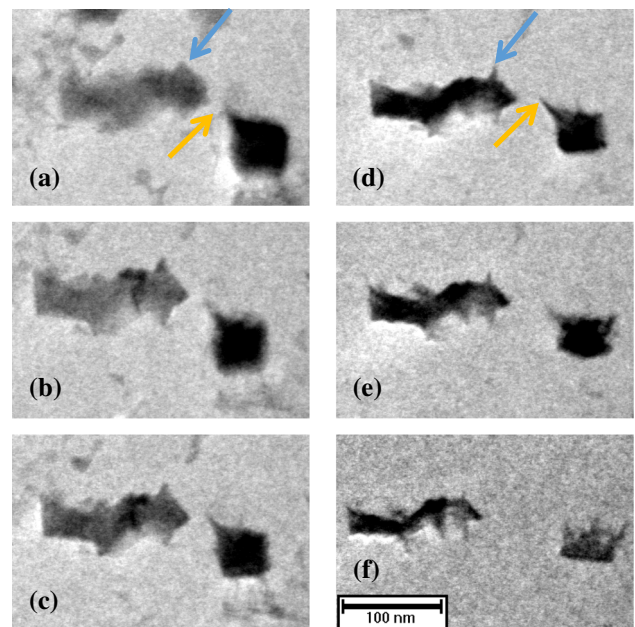


**Figure 2** Generation and transformation of needle-shaped particles. Case 2: Formation of needles oriented on specific facets relative to the particles. Timings for the frames are (setting a to 0 s): b 5.8 s, c 6.7 s, d 12.7 s, e 15.1 s, f 22.4 s.

and therefore the dissolution rate of needles must be slower than that of ceria nanoparticles. Eventually, all solid phase dissolves (as reported in [21]).

In a related observation, “case 3”, multiple needles were observed forming in some cases star-shaped multi-spike structures out of solid particles. In Fig. 3, these highly transient structures, reaching best visibility in Fig. 3b, seem to consume eventually all of the parent particles with small spikes receding in favour of one dominant spike, resulting eventually in a

single needle (Fig. 3d). The most clearly visible particle cluster is encircled in blue in Fig. 3. Further irradiation then dissolves also the last needle.

### Formation of necks and bridges

Beyond spike-shaped particles, particular interest is in needles connecting between two neighbouring pre-existing particles. This can be observed either as short connections of two corners forming a neck or by longer “bridges” which appear identical to the earlier identified spikes, except that they connect simultaneously two suitably oriented particle facets. Finally, the idea of neck or bridge formation, if iterated, will lead to particle chains. In Figs. 4, 5, we expand on this phenomenon by listing various remarkable examples for needle-like phases connecting two or more neighbouring (mostly octahedral) ceria nanoparticles.

The first example in Fig. 4a shows a short connection of two cube–octahedral ceria nanoparticles, imaged sharply through little water thickness. Here the needle-shaped neck can be clearly identified to connect both octahedra at {100} cube facets, and both ceria nanoparticles are aligned with common octahedral symmetry axes. Similarly, however blurred by larger water thickness, the cases of Fig. 4b, c show firstly a straight bridge connecting two corners,

however with the two c-axes of ceria nanoparticles not perfectly parallel (Fig. 4b) or a “bent” double-bridge connecting two large ceria nanoparticles via an intermediate small ceria nanoparticle (Fig. 4c). Finally, Fig. 4d, e underpins the impression of such bridges being a common phenomenon on multiple neighbouring particle systems. Here the needle decoration of two perpendicular {100}-facet directions leads to a network of particles co-oriented via intermediate needles at 90° (Fig. 4e), or at later stages (when most of the original particles vanish) to the formation of “chains of needles” (Fig. 4f).

On another occasion, Fig. 5, a video sequence of failure (presumably by rupture) of one bridge could be observed. The continuation of this sequence (Fig. 5d–f) is interesting as it comprises a switch from a corner docking (Fig. 5d, blue arrow) into a face-on-face attachment (Fig. 5e, f, yellow arrow) upon forming of a little chain. The latter sequence (Fig. 5d–f), however, happens at a time when dissolution of the raw particles is already showing strongly.

### Formation of chains

The driving force of particle attachment, presumably electrostatic, is clearly long range as imaged in Fig. 6, where pre-existing pairs of particles coagulate over

**Figure 3** Generation and transformation of needle-shaped particles. Case 3: multiple needles per host particle form into star-shaped objects (blue circled object discussed in the text), followed by narrowing of needles and ultimately dissolution.

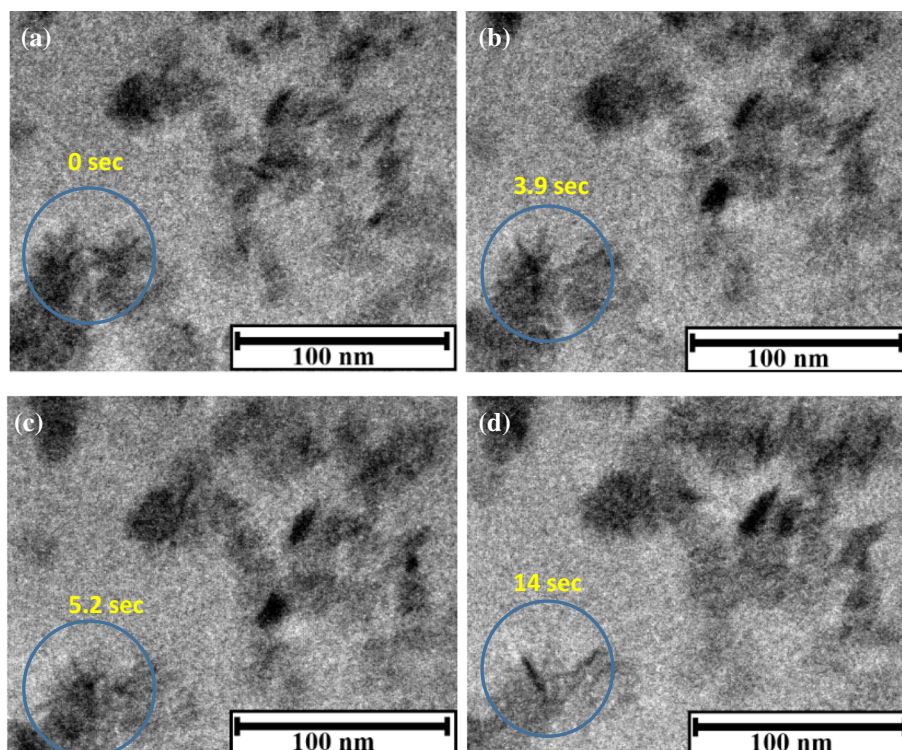


**Figure 4** Neck and bridge formation (yellow arrows) between neighbouring ceria nanoparticles as temporary features within a longer term dissolution process of the particles. **a–c** Are snapshots of three different regions. **d–e** Orientation of multiple perpendicular needle features on cube–octahedral  $\{100\}$  facets, and suggested model morphology as blue sketches. **f** Chain of rod type attachment at advanced stages of dissolution.

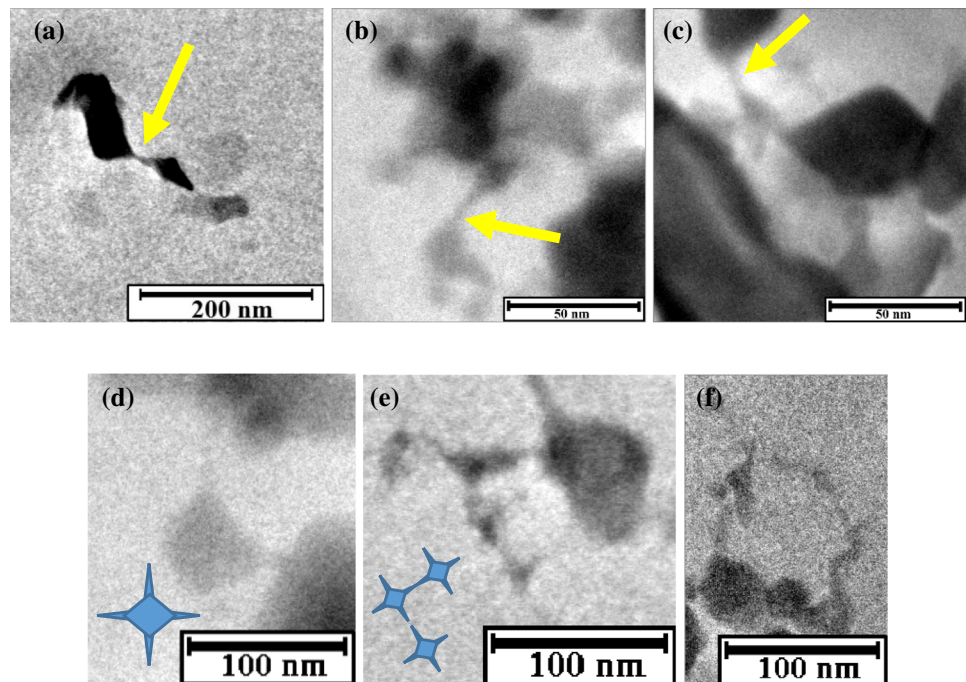
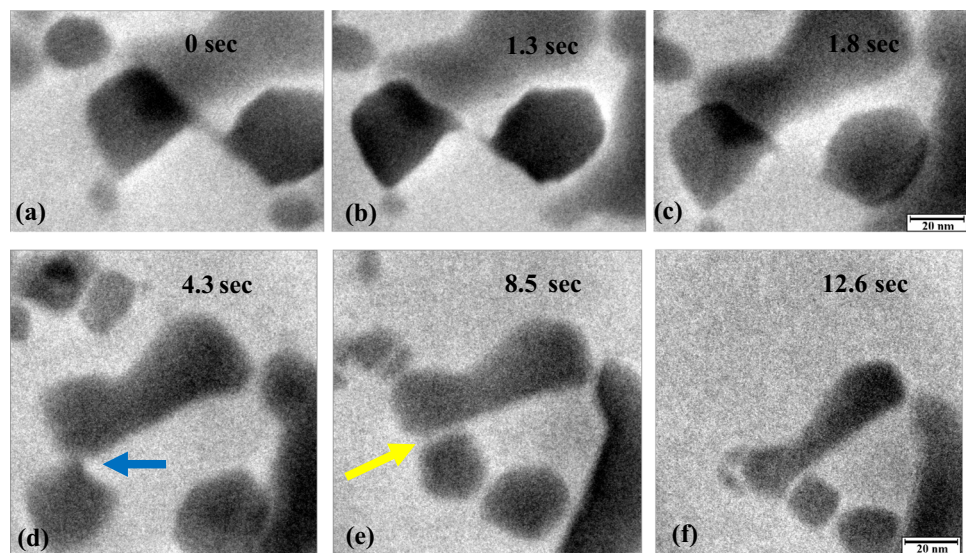


**Figure 5** **a–c** Sequence of rupture of bridge between two ceria octahedra. **d–f** Transition from corner docking of octahedra to flat-facet attachment and formation of a small chain. Docking locations with blue and yellow arrows, as discussed in the text.



distances a multiple of their diameter to form particle chains with 3–8 members. In the first example (Fig. 6a–c) the original touching point is again a corner of cube–octahedron (red arrow) although the attachment remains flexible for bending movements. The second sequence is about straightening a zig-zag chain (Fig. 6d) into a five-particle chain (Fig. 6e), which eventually breaks up, indicating that there is competition between particle–particle and particle–membrane (Si-nitride) attractions.

In contrast to the in situ formation of particle chains as of Figs. 5 and 6, there are also some cases of likely ex situ formed octahedral ceria nanoparticle chains, pre-existing before irradiation. The in situ irradiation sequence then shows the chain to turn into one major nanorod of longer size than the original particles (Fig. 7).

Formations of longer particle chains, not involving needles or visible attachment sites, are also found (Fig. 8). The particles appear roundish due to high water thickness and smaller magnification used. In

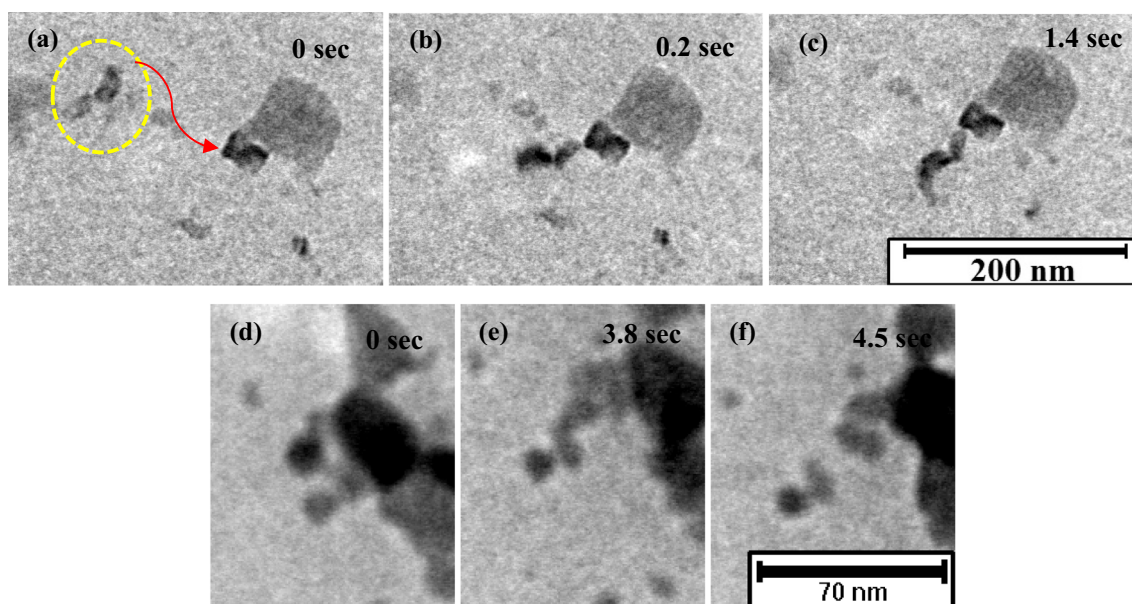


**Figure 6** a–c Long-range particle jumps to form larger clusters initially docking at corners. d–f In situ formation of a chain (d–e) of octahedral nanoparticles and its rupture (e–f).

building this chain, particles appear to be collected from a rather large distance, and all particles entering the chain have a rather mono-disperse size distribution. A final conversion of the particle chain into a needle or rod does not happen in this case, separating it from the previous examples.

## Discussion

The observations on the in situ formation of 1D-nanostructures are sorted into 3 aspects/categories, which are, however, considered interrelated:

- (i) Formation of single-particle needle-shaped nanostructures (Fig. 1)
- (ii) Multi-particle assemblies involving needle shapes on pre-existing nanoparticles, such as star-shapes (Figs. 2, 3)

- (iii) Particle chains, including chain formation from isotropic particles or chains of needles (Figs. 4, 5, 6, 7, 8)

### About aspect (i), single needle-shaped particles

Possible cerium-rich compound structures which are known to exhibit rod or needle shape include the four cases of cubic  $\text{CeO}_2$ , hexagonal  $\text{Ce}_2\text{O}_3$ , hexagonal  $\text{Ce}(\text{OH})_3$ , and cubic  $\text{Ce}(\text{OH})_4$ . The two hexagonal cases would lend themselves most easily to needle shape growth through crystallographic anisotropy, as they have unique axes, distinct from any other direction.  $\text{Ce}(\text{OH})_3$  nanorods (known to be more stable as a solid than  $\text{Ce}(\text{OH})_4$ ) are reported in TEM-research, e.g. Ma et al. [26], although considered not air stable, while round  $\text{Ce}(\text{OH})_3$  particles are found in

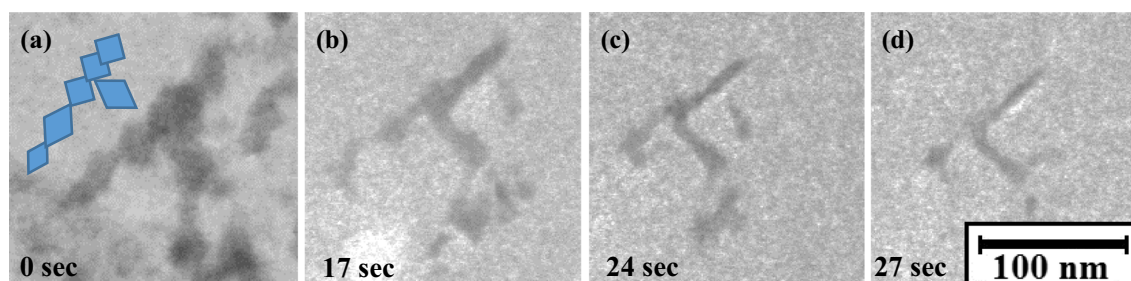


**Figure 7** Chain-of-octahedra shape transformation into nanorod larger than raw particles. Indicative original structure symbolised in blue.

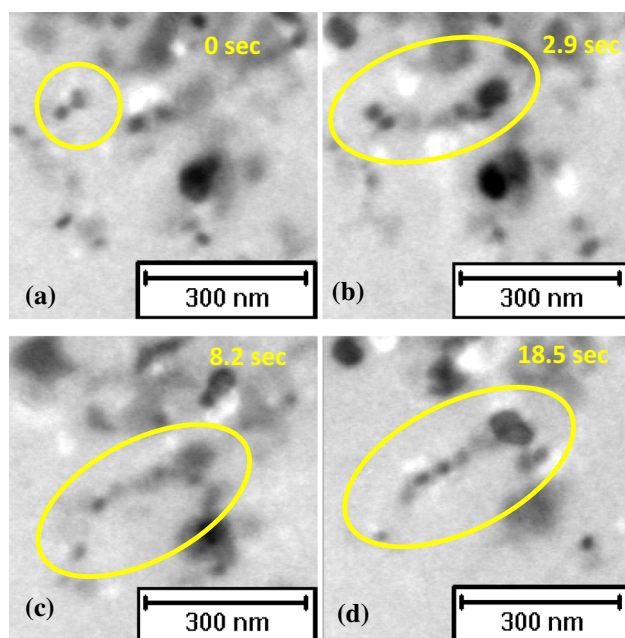


**Figure 8** Particle-chain formation and alteration: Case of roundish particle morphologies. Formation of nanoparticle pairs (a) followed by multi-particle chains (b–d) under electron irradiation.

Abellan et al. [27].  $\text{Ce}_2\text{O}_3$  reductive reaction products are known in TEM, but have never been reported to be of needle shape.  $\text{Ce}(\text{OH})_4$  is sometimes treated as a hydrated variety of  $\text{CeO}_2$ , however, its observation as solid needles is rare and on one occasion has been linked to specific growth conditions and use of surfactants [28] only. The fact that no needle shapes have ever been found on disassembled dry  $\text{Si}_3\text{N}_4$  chips indicates instability of the needle phase.

On the other hand cubic  $\text{CeO}_2$  has been reported to grow into rod and needle shape, in spite of its cubic symmetry, by one of two possible mechanisms: (i)  $\text{CeO}_2$ -nanorods might convert from intermediate  $\text{Ce}(\text{OH})_3$  nanorods, which form a template, by hydrothermal or airborne oxidation or special ageing procedures [29, 30]; (ii) oxide nanorods have been imaged to form directly by “oriented attachment” of preformed ceria nanoparticles oriented in either  $\langle 110 \rangle$  or  $\langle 211 \rangle$  growing direction for the rod [8, 31]. For  $\text{CeO}_2$  cube–octahedral attachments along  $\langle 100 \rangle$ , matching our observations, theoretically calculated predictions exist [32].

The crystalline nature of the rods is unambiguously confirmed via Bragg scattering induced double images, displaced from the particles due to defocus

and lens aberrations; see Fig. 9. These would not exist for amorphous material phases.

In a related case, for cubic PdSe nanoparticles, oriented attachment growth in  $\langle 100 \rangle$  direction has been found [33], and motivated by a collective  $\langle 100 \rangle$ -directed dipole moment originating from multiple dipoles on various  $\{100\}$  facets of cuboctahedral particles with rocksalt structure.

### About aspect (ii), spiked particles and bridges between particles

This aspect is about the relative orientations between needles and (octahedral) pre-existing particles: In the cases highlighted in the figures, the needle orientation relative to the mirror planes of the original particles is compatible to what is a cubic  $\{100\}$  ceria nanoparticle plane normal. That renders an epitaxial growth of hexagonal rods (in whatever direction) on cubic planes unlikely due to symmetry mismatch. Growth of  $\text{Ce}(\text{OH})_4$  needles cube-on-cube would avoid symmetry mismatch, however, the factor 2 in Ce:O ratio between  $\text{CeO}_2$  and  $\text{Ce}(\text{OH})_4$  should result in visible grey-value change on our TEM images from NPs to rods, which is never observed (e.g. see Figs. 1, 2, 3).

Instead, epitaxial bridges of the kind of Figs. 4 and 7 resemble a specific type of ceria nanoparticle aggregation found sometimes in original, un-irradiated powders observed by standard (dry) TEM. The main difference to the liquid-cell TEM is that the “neck” between two crystals would be pre-thinned and elongated by radiolytic water-induced dissolution. Such a separately recorded dry TEM image (aberration corrected HRTEM) is shown for illustrative purpose as Fig. 10.

Here, ceria nanoparticle powder represented by a randomly found cluster of predominantly octahedra ceria nanoparticles shows clear epitaxial attachment on  $\{100\}$  planes with atomically sharp bonding, turning the entire cluster into a “single crystal”. If the attachment direction would be along a common  $[001]$  direction, this matches  $\langle 001 \rangle$  “oriented attachment” (as labelled “case i” in Zhang and Banfield [32], see also [34] for the case of chains made of anatase  $\text{TiO}_2$ ). Molecular modelling simulated self-assembly of ceria nanooctahedra is described in Kuchibhatla et al. [35]. The new needle phase appears rigid enough to survive mechanical tension until fracture (Fig. 5), rather than de-attaching from the docking

**Figure 9** Bright-field-dark-field pairs of needle shapes translated through aberrations (yellow arrows), indicating crystallinity through Bragg reflection.

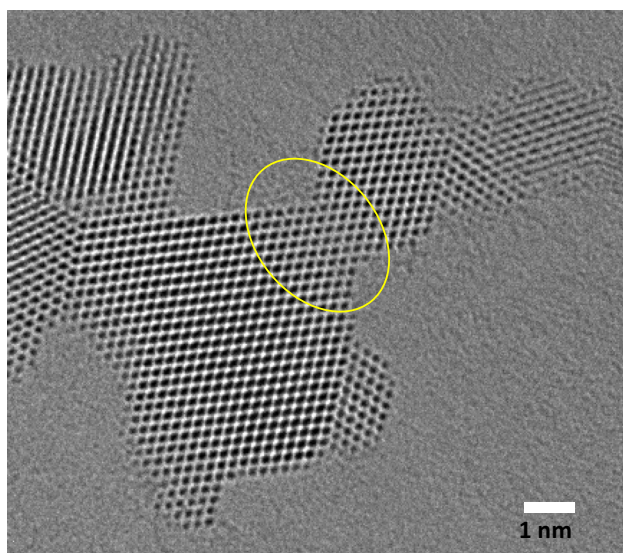
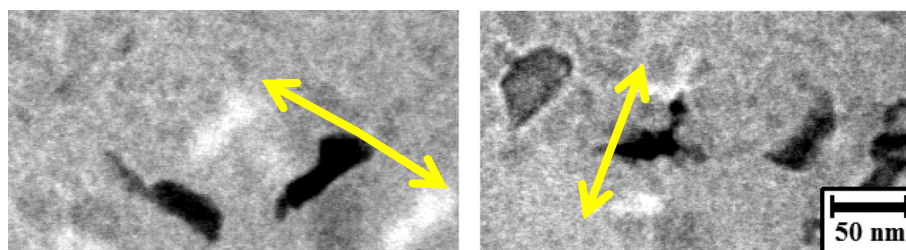


**Figure 10** Dry-TEM equivalent observation of static “necks” in ceria nanoparticle chain formation by aggregation along [100] (Sheffield-JEM 3100 R005).

position on the ceria nanoparticles, indicating strong bonds between needles and cube-octahedral surface facets.

Another important consideration is the principle of particle “envelope”: This concept evaluates whether any new 1D structure (needles, spikes, stars) forms inside or outside the external frame (envelope) of the old particle before irradiation:

Measurements on Fig. 2 reveal that the new spiky particle entirely fits within the envelope of the original particle. Such a process would peculiarly maximise surface energy by depleting the most energetically favourable ceria facets first. Therefore, this can only happen if an overruling driving force exists, such as a phase transformation, which prefers 1D rod shape as a new morphology. On the other hand, in the examples of Figs. 4 and 7, 1D rods or bridges comprise and consume multiple raw particles, and therefore form outside the envelope of any raw particle. The complexity of the system is further enhanced, as the timing of spike or bridge formation

as of Figs. 2, 3, 4, 5, 6, 7 is rather late during an entire ceria-dissolution video-recording sequence, and the chemical identity of the particles from which the needles form, might no longer be considered chemically stoichiometric CeO<sub>2</sub>.

Finally, we refer to similarity of bent bridges (Fig. 4b, c) to the case of “near-oriented attachment” introduced in Yoreo et al. [36] and furthermore to the case of formation of “Mineral Bridges” as one of four mechanisms of oriented attachment growth as discussed in Song and Cölfen [37].

### About aspect (iii), particle chain formation

Finally, we contrast the atomically sharp attachment of above aspect (ii) with the more commonly observed “loose” attachment of two particles on corners or faces during live video-recording, with orientation relationship remaining flexible as of Fig. 6 and 8. In this aspect (iii), the driving force for attraction is mainly expected to be a result of surface charges with field lines connecting the tips or spikes of neighbouring particles, not forming any chemical bond. Formation of particle chains or rod chains would minimise the free surface charge and stray field energies. Within liquid cell TEM research, chain-forming behaviour has been found for metallic NPs, such as Fe<sub>3</sub>Pt [38] or Au [39] and motivated either by magnetic dipole interactions or electrostatic interactions. For Au nanoparticles, pair formation with a small equilibrium distance between non-touching particles has been described [11], with a balance struck between attractive van der Waals forces and repulsive hydration double-layer forces, while entire Au nanorod chains are found in [40] with an end-to-end local van der Waals attachment proposed after irradiation had weakened electrostatic repulsive forces. The particle–particle finite distance is considered transient before atomistic bonds eventually form, as observed in liquid cell TEM in [11]. Furthermore, it is highly likely that all particles in the chain are

attached to the underlying  $\text{Si}_3\text{N}_4$  membrane and merely move in 2D. For ceramic nanoparticulate materials, e.g. in the ZnO or ZnS family, Wurtzite structure would contribute a natural orientational asymmetry. However, for the cubic sphalerite modification, net dipole moments have been identified to be necessary to be generated by surface occupancy defects, or subtle shape asymmetries [41]; furthermore, embedding in water is shown to strengthen dipole moments [41]. For fluorite instead of sphalerite, the [100] facets contribute unsaturated dipoles on the nanoscale even in the absence of water. Once a dipole moment is established, electric field interaction along the axis of a particle pair forces the 3rd particle on line [12] rather than in a close-packed position, which would be expected [42] in a general 2D colloidal particle assembly.

As the attachment events in this work happen alongside overall corrosive dissolution [21], we remind of earlier examinations, including dry irradiation [43] finding a “robust” (irradiation resistant and mechanically rigid) cerium oxide fluorite structure, which would exclude the formation of necks/bridges using diffusion and surface flow. Equivalently, radiation-induced fluidity or “quasi-melting”, as examined in glasses and ceramics, is un-realistic for liquid cell TEM, as most beam energy is absorbed by the water and the  $\text{Si}_3\text{N}_4$  membranes.

The question when or whether particles during dissolution adopt rounding to a sphere (as found in Asghar et al. [21]), elongation from isotropic to oval form (as found in Asghar et al. [22]), or ultimately conversion to needle shape, as reported here, must be due to timing, as there is no deliberate change in sample geometry, liquid, or particle loading. Different amounts of pre-exposure to electrons will alter local pH and water dissociation products, and formation of surface reaction layers on raw particles. The option that any needle shapes are already in existence on the raw nanoparticles can be safely excluded due to our extensive studies of the dry particles [24, 25, 44].

## Conclusions

It has been shown that real-time video-rate observation by liquid-cell TEM is a powerful technique to gain new insight into radiation-induced chemistry changes of cerium oxide particles in radiolytic water

environment. Growth of a variety of needle or rod shaped morphologies around original ceria nanoparticles including formation of particle chains is found. The attachment is a combination of two bond types: (i) electrostatic, water-mediated, interactions between pairs or chains of particles remaining mobile with bending degree-of-freedom, and (ii) crystallographic surface (e.g. dipole) specific interactions on chemical bond level to achieve a rigid attachment and crystallographic preference in growth axes. For both cases, the small {100} facelets of cuboctahedra seem to be the preferential site. The needles as well as the original particles are unstable against dissolution as long as high-intensity electron irradiation is ongoing.

## Acknowledgements

We thank EPSRC, UK (EP/J021199/1), NED University of Engineering and Technology Karachi, Pakistan, and The University of Sheffield, UK, for funding parts of this project, as well as Dr U Bhatta and Dr I Ross for help with the micrograph of Fig. 10.

**Open Access** This article is distributed under the terms of the Creative Commons Attribution 4.0 International License (<http://creativecommons.org/licenses/by/4.0/>), which permits unrestricted use, distribution, and reproduction in any medium, provided you give appropriate credit to the original author(s) and the source, provide a link to the Creative Commons license, and indicate if changes were made.

## References

- [1] Sun C, Liab H, Chen L (2012) Nanostructured ceria-based materials: synthesis, properties, and applications. *Energy Environ Sci* 5:8475–8505
- [2] Celardo I, Pedersen JZ, Traversa E, Ghibelli L (2011) Pharmacological potential of cerium oxide nanoparticles. *Nanoscale* 3:1411–1420
- [3] Gorte RJ (2010) Ceria in catalysis: from automotive applications to the water-gas shift reaction. *AIChE J* 56(5):1126–1135
- [4] Zhou F, Zhao X, Xu H, Yuan C (2007)  $\text{CeO}_2$  spherical crystallites: synthesis, formation mechanism, size control, and electrochemical property study. *J Phys Chem C* 111:1651–1657

- [5] Zhang F, Jin Q, Chan S-W (2004) Ceria nanoparticles: size, size distribution, and shape. *J Appl Phys* 95(8):4319–4326
- [6] Wang W, Howe JY, Li Y, Qiu X, Joy DC, Paranthaman MP, Doktycz MJ, Gu B (2010) A surfactant and template-free route for synthesizing ceria nanocrystals with tunable morphologies. *J Mater Chem* 20:7776–7781
- [7] Lin K-S, Chowdhury S (2010) Synthesis, characterization, and application of 1-D cerium oxide nanomaterials: a review. *Int J Mol Sci* 11:3226–3251
- [8] Ji Z, Wang X, Zhang H, Lin S, Meng H, Sun B, George S, Xia T, Nel AE, Zink JI (2012) Designed synthesis of CeO<sub>2</sub> nanorods and nanowires for studying toxicological effects of high aspect ratio nanomaterials. *ACS Nano* 6(6):5366–5380
- [9] Talapin DV, Murray CB (2005) PbSe nanocrystal solids for *n*- and *p*-channel thin film field-effect transistors. *Science* 310(5745):86–89
- [10] Karakoti AS, Das S, Thevuthasan S, Seal S (2011) Pegylated inorganic nanoparticles. *Angew Chem Int Ed* 50:1980–1994
- [11] Anand U, Lu J, Loh D, Aabdin Z, Mirsaidov U (2016) Hydration layer-mediated pairwise interaction of nanoparticles. *Nano Lett* 16:786–790
- [12] Sinyagin AY, Belov A, Tang Z, Kotov NA (2006) Monte carlo computer simulation of chain formation from nanoparticles. *J Phys Chem B* 110:7500–7507
- [13] Vincent A, Inerbaev TM, Babu S, Karakoti AS, Self WT, Masunov AE, Seal S (2010) Tuning hydrated nanoceria surfaces: experimental/theoretical investigations of ion exchange and implications in organic and inorganic interactions. *Langmuir* 26(10):7188–7198
- [14] Goi D, Leitenburg CD, Dolcetti G, Trovarelli A (2006) COD and AOX abatement in catalytic wet oxidation of halogenated liquid wastes using CeO<sub>2</sub>-based catalysts. *J Alloy Compd* 408(412):1136–1140
- [15] Paier J, Penschke C, Sauer J (2013) Oxygen defects and surface chemistry of ceria: quantum chemical studies compared to experiment. *Chem Rev* 113:3949–3985
- [16] Molinari M, Parker SC, Sayle DC, Islam MS (2012) Water adsorption and its effect on the stability of low index stoichiometric and reduced surfaces of ceria. *J Phys Chem C* 116:7073–7082
- [17] Williamson MJ, Tromp RM, Vereecken PM, Hull R, Ross FM (2003) Dynamic microscopy of nanoscale cluster growth at the solid-liquid interface. *Nat Mater* 2(8):532–536
- [18] Chen F-C, Chen J-Y, Lin Y-H, Kuo M-Y, Hsu Y-J, Wen-Wei W (2019) In situ TEM observation of Au–Cu<sub>2</sub>O core-shell growth in liquids. *Nanoscale* 11(21):10486–10492
- [19] Kim SY, Dae KS, Koo K, Kim D, Park J, Yuk JM (2019) Sequential growth and etching of gold nanocrystals revealed by high-resolution liquid electron microscopy. *Phys Status Solidi A* 216:1800949
- [20] Krans NA, Ahmad N, Alloye D, de Jong KP, Zečević J (2019) Attachment of iron oxide nanoparticles to carbon nanofibers studied by insitu liquid phase transmission electron microscopy. *Micron* 117:40–46
- [21] Asghar MSA, Inkson B, Seal S, Molinari M, Sayle D, Möbus G (2018) In-situ observation of radiation physics and chemistry of nanostructured cerium oxide in water. *Mater Res Express* 6(1):015032
- [22] Asghar MSA, Inkson B, Möbus G (2017) Giant radiolytic dissolution rates of aqueous ceria observed insitu by liquid-cell TEM. *ChemPhysChem* 18(10):1247–1251
- [23] Klein KL, Anderson IM, de Jonge N (2011) Transmission electron microscopy with a liquid flow cell. *J Microsc* 242:117–123
- [24] Bhatta UM, Reid DL, Sakthivel T, Sayle TXT, Sayle DC, Molinari M, Parker SC, Ross IM, Seal S, Möbus GN (2013) Morphology and surface analysis of pure and doped cuboidal ceria nanoparticles. *J Phys Chem C* 117:24561–24569
- [25] Xu X, Saghi Z, Gay R, Möbus G (2007) Reconstruction of 3D morphology of polyhedral nanoparticles. *Nanotechnology* 18(22):225501
- [26] Ma Y, Gao W, Zhang Z, Zhang S, Tian Z, Liu Y, Ho JC, Qu Y (2018) Regulating the surface of nanoceria and its applications in heterogeneous catalysis. *Surf Sci Rep* 73:1–36
- [27] Abellan P, Moser TH, Lucas IT, Grate JW, Evans JE, Browning ND (2017) The formation of cerium(III) hydroxide nanoparticles by a radiation mediated increase in local pH. *RSC Adv* 7(7):3831–3837
- [28] Tang K, Zhang J, Wang W, Wang S, Guo J, Yang Y (2015) Construction of Ce(OH)<sub>4</sub> nanostructures from 1D to 3D by a mechanical force-driven method. *Cryst Eng Commun* 17:2690–2697
- [29] Sakthivel T, Das S, Kumar A, Reid DL, Gupta A, Sayle DC, Seal S (2013) Morphological phase diagram of biocatalytically active ceria nanostructures as a function of processing variables and their properties. *Chem Plus Chem* 78:1446–1455
- [30] Sakthivel TS, Reid DL, Bhatta UM, Möbus G, Sayle DC, Seal S (2015) Engineering of nanoscale defect patterns in CeO<sub>2</sub> nanorods via ex situ and in situ annealing. *Nanoscale* 7:5169–5177
- [31] Du N, Zhang H, Chen B, Ma XA, Yang D (2007) Ligand-free self-assembly of ceria nanocrystals into nanorods by oriented attachment at low temperature. *J Phys Chem C* 111:12677–12680
- [32] Zhang H, Banfield FF (2012) Energy calculations predict nanoparticle attachment orientations and asymmetric crystal formation. *J Phys Chem Lett* 3:2882–2886
- [33] Cho K-S, Talapin DV, Gaschler W, Murray CB (2005) Designing PbSe nanowires and nanorings through oriented

- attachment of nanoparticles. *J Am Chem Soc* 127:7140–7147
- [34] Penn RL, Banfield JF (1999) Morphology development and crystal growth in nanocrystalline aggregates under hydrothermal conditions: insights from titania. *Geochim Cosmochim Acta* 63(10):1549–1557
- [35] Kuchibhatla SVNT, Karakoti AS, Sayle DC, Heinrich H, Seal S (2009) Symmetry-driven spontaneous self-assembly of nanoscale ceria building blocks to fractal superoctahedra. *Cryst Growth Des* 9(3):1614–1620
- [36] Yoreo JJD, Gilbert PUPA, Sommerdijk NAJM, Penn RL, Whitelam S, Joester D, Zhang H, Rimer JD, Navrotsky A, Banfield JF, Wallace AF, Michel FM, Meldrum FC, Cölfen H, Dove PM (2015) Crystallization by particle attachment in synthetic, biogenic, and geologic environments. *Science* 349(6247):1–10
- [37] Song RQ, Cölfen H (2010) Mesocrystals-ordered nanoparticle superstructures. *Adv Mater* 22(12):1301–1330
- [38] Powers AS, Liao H-G, Raja SN, Bronstein ND, Alivisatos AP, Zheng H (2017) Tracking nanoparticle diffusion and interaction during self-assembly in a liquid cell. *Nano Lett* 17:15–20
- [39] Verch A, Pfaff M, Jonge ND (2015) Exceptionally slow movement of gold nanoparticles at a solid/liquid interface investigated by scanning transmission electron microscopy. *Langmuir* 31(25):6956–6964
- [40] Chen Q, Cho H, Manthiram K, Yoshida M, Ye X, Alivisatos AP (2015) Interaction potentials of anisotropic nanocrystals from the trajectory sampling of particle motion using in situ liquid phase transmission electron microscopy. *ACS Cent Sci* 1:33–39
- [41] Shanbhag S, Kotov NA (2006) On the origin of a permanent dipole moment in nanocrystals with a cubic crystal lattice: effects of truncation, stabilizers, and medium for CdS tetrahedral homologues. *J Phys Chem B* 110(25):12211–12217
- [42] Talapin DV, Shevchenko EV (2007) Dipole-dipole interactions in nanoparticle superlattices. *Nano Lett* 7(5):1213–1219
- [43] Bhatta UM, Karounis F, Stringfellow A, Möbus G (2013) Perforation and carbon ablation experiments on nano-ceria by electron irradiation. *MRS Proc* 1552:125–130
- [44] Möbus G, Saghi Z, Sayle DC, Bhatta UM, Stringfellow A, Sayle TXT (2011) Dynamics of polar surfaces on ceria nanoparticles observed in situ with single-atom resolution. *Adv Funct Mater* 21:1971–1976

**Publisher's Note** Springer Nature remains neutral with regard to jurisdictional claims in published maps and institutional affiliations.